NJC

High Tg fluoranthene-based electron transport materials for organic light-emitting diodes

Journal:	*New Journal of Chemistry*
Manuscript ID:	NJ-ART-03-2015-000750.R2
Article Type:	Paper
Date Submitted by the Author:	29-May-2015
Complete List of Authors:	Patil, Satish; Indian Institute of Science, Solid State and Structural Chemistry Unit Kumar, Shiv; Indian Institute of Science, SSCU

Journal Name

ARTICLE

High Tg fluoranthene-based electron transport materials for organic light-emitting diodes†

Received 00th January 20xx,
Accepted 00th January 20xx

DOI: 10.1039/x0xx00000x

www.rsc.org/

Shiv Kumar[a] and Satish Patil[a*]

In this work, fluoranthene-based derivatives with a high thermal stability are synthesized for applications in organic electroluminescent devices. The two derivatives synthesized in this work, bis(4-(7,9,10-triphenylfluoranthen-8-yl)phenyl)sulfane (**TPFDPS**) and 2,8-bis(7,9,10-triphenylfluoranthen-8-yl)dibenzo[b,d]thiophene (**TPFDBT**), were characterized by cyclic voltammetry, differential scanning calorimetry (DSC) and thermogravometric analysis (TGA). TPFDPS exhibits high T_g of 210 °C while TPFDBT is crystalline in nature. Both the derivatives are thermally stable up to 500°C. The charge transport studies reveal predominant electron transport properties. Subsequently, we fabricated blue OLEDs with 2-tert-butyl-9,10-bis-(β-naphthyl)-anthracene (**TBADN**) as emitting layer to demonstrate the applications of these molecules as an electron transporting layer.

Introduction

The pioneering work of Tang and VanSlyke results into tremendous activity to improve the performance of fluoroscent-based organic light-emitting diode (OLED). OLED have continued to attract interest both from scientific and industrial community because of their promising applications in low-cost, flat-panel, full-color display technology and solid state lighting.[1-3] The presence of vast literature on OLEDs is the evidence of the ongoing scientific efforts to design and synthesize thermally robust emitting and charge transport materials for development of the next generation high performance OLEDs based on small molecules and polymers.[4, 5] In this context, development of hole and electron transporting layers has earned considerable attention. In 1995, Strukelj *et al* proposed the rational design and application of electron-transporting organic materials.[6] Thereafter, several kinds of electron transport materials (ETMs) including oxadiazole derivatives,[7-9] metal chelates,[1, 10, 11] azole-based materials,[12] triazines,[13] 1,3,5-tris(N-phenylbenzimidizol-2-yl)benzene (TPBI),[14] pyridine-based materials,[15] quinoxaline-based materials,[16, 17] phenanthrolines,[18, 19] perfluorated materials,[20, 21] dimesitylboryl moieties,[22] oligothiophene-S,S-dioxides,[23] and dibenzothiophene-5,5-dioxide[24] were explored. The glass transition temperature (T_g) of these materials ranges from 60-200 °C. On the other hand, the ETMs such as polybenzobisazoles,[25] octasubstituted cyclooctatetraenes (COTs),[26] and quinoline-based materials[27] exhibit T_g >200 °C. Kulkarni *et al* speculated that all the ETMs for OLEDs should have a high glass transition temperature (T_g), preferably greater than 150 °C to improve durability of the devices, irrespecitive of emission region.[5] Also, it has been observed that the thermally robust ETMs with T_g >200 °C give a very stable repeatable performance in OLEDs, whereas the ETMs with T_g <90 °C degrade with high electric field due to melting/crystallization of ETM layer.[28] Increasing the molecular weight and chain rigidity is the most effective strategy to enhance the thermal stability (T_g) of ETM as well as the processibility (solution-processibility).[29] Most recently, Wang *et al* reported low-cost phenylbenzoimidazole derivative (T_g 139 °C) as an alternative ETM to TPBI (T_g 124 °C).[30] Shih *et al* synthesized m-terphenyl oxadiazole derivatives as universal electron-transporting/exciton-blocking materials (T_gs ~80-105 °C) for phosphorescent OLEDs.[31] Although the devices exhibited reduced driving voltages, very high efficiency and negligible roll-off, but the thermal stability of ETMs is still a major concern limiting the further development of OLED. In an effort to address this problem, we have synthesized fluoranthene based materials and explored as an electron transporting layer in OLED.

Fluoranthene is a cyclopentene-fused polycyclic aromatic hydrocarbon, and its chemical structure was elucidated by Whalley et al. in 1952.[32] Due to unique chemical structure, fluoranthene has been studied extensively for its anomalous photophysical properties.[33, 34] Along with the theoretical study of fluoranthene and its derivatives, efforts have been put to develop the facile synthesis of fluoranthene derivatives.[35] Because of the rigid fluoranthene core, its derivatives are well known for their wide energy gap, high photoluminescence quantum yield (PLQY), thermal and electrochemical stability.[36, 37] Above mentioned properties make the fluoranthene derivatives as potential candidate for fluorescent materials for

[a] *Solid State and Structural Chemistry Unit, Indian Institute of Science, Bangalore, India.*
E-mail: satish@sscu.iisc.ernet.in Ph: +91-80-2293-2651
† Electronic Supplementary Information (ESI) available: ^{1}H & ^{13}C NMR spectra, MS (MALDI-TOF) spectra, CIE 1931 chromaticity plot. See DOI: 10.1039/x0xx00000x

OLEDs.[38-40] Apart from emitting materials for OLEDs, fluoranthene derivatives were also explored as efficient electron-acceptor materials for photovoltaics.[41] In this work, we designed and synthesized two fluoranthene derivatives, bis(4-(7,9,10-triphenylfluoranthen-8-yl)phenyl)sulfane (TPFDPS) and 2,8-bis(7,9,10-triphenylfluoranthen-8-yl)dibenzo[b,d]thiophene (TPFDBT); as electron transporting materials for organic light-emitting diodes.

Experimental Section

Materials

1-Bromo-4-iodobenzene, dibenzothiophene, phenylacetylene, copper (I) iodide, and tetrakis(triphenylphosphine)palladium (0) were purchased from Sigma-Aldrich co. and used directly without further purification. Chloroform was distilled over phosphorus pentoxide prior to use. Toluene was distilled over sodium/benzophenone under argon atmosphere. Diisopropylamine was distilled over sodium hydroxide prior to use.

Characterization

All the derivatives were confirmed with NMR spectroscopy, mass spectrometry and elemental analysis. ^{1}H and ^{13}C NMR spectra were recorded on Bruker 400 MHz and 100 MHz spectrometer, respectively, $CDCl_3$ as solvent and calibrated using TMS as an internal reference. Chemical shifts are reported in parts per million (ppm). Mass spectra were recorded on Thermo LCQ Deca XP Max by electrospray ionization (ESI) technique. Elemental analysis was carried out on Thermo Scientific Flash 2000 Organic Elemental Analyzer. The UV-visible absorption spectra were obtained with a Perkin-Elmer (Lambda 35) UV-visible spectrometer. All the absorption spectra in the solution state were recorded in optical grade chloroform (conc. $1x10^{-5}$ M), and the spectra in solid state were recorded from films of compounds spin coated on quartz substrate. Steady-state fluorescence emission spectra were recorded on Horiba Jobin-Yvon FluoroLog-3 spectrometer. The transient PL decay characteristics were recorded with time correlated single photon counting (TCSPC) method using LED 365 nm with a Quantaurus-Tau fluorescence lifetime measurement system (C11367-03, Hamamatsu Photonics Co.). The fluorescence emission decay was well fitted by a single exponential decay profile. Absolute photoluminescence quantum yields (PLQY) were obtained using a Quantaurus-QY measurement system (C11347-11, Hamamatsu Photonics Co.). Thermo-gravimetric analysis (TGA) was carried out using a Diamond TG/DTA instrument under a nitrogen atmosphere by measuring the weight loss during heating from 25 to 600 °C at a rate of 10 °C/min. Differential Scanning Calorimetry (DSC) analysis was carried out on Mettler Toledo DSC1 STARe system (chiller cooled) with N_2 flow of 40 mL/min with an empty Al pan taken as standard. All samples were heated up at a heating rate of 10 °C/min. Redox potentials were determined by cyclic voltammetry (CV) experiment using CH electrochemical analyser with a scanning rate of 50 mV/s. Synthesized materials (0.2 mg/ 0.1 mL in DCM) were drop casted on the working Pt disc electrode. Ag/AgCl was used as a reference electrode whereas Pt wire was employed as counter electrodes. Dry chloroform and 0.1 M tetrabutylammonium hexafluorophosphate were used as solvent and supporting electrolyte, respectively. Ferrocene/ferrocenium (Fc/Fc^{+}) couple was used as standard electrochemical reference.[42]

Device fabrication and measurement

After the pre-cleaned indium tin oxide (ITO) glass substrates were treated with ozone for 15 min, a 60 nm thick TPD layer, a 10 nm TBADN layer and a 40 nm thick layer of ETM were deposited consecutively on the substrates in an inert chamber under a pressure of $<4\times10^{-4}$ Pa. Finally, the cathode was fabricated by thermal evaporation of a LiF layer (1.0 nm), followed by an Al layer (100 nm). The deposition rates of the organic layers and the Al layer were 0.1-0.2 nm/s, while that of the LiF layer was 0.1 Å/s. The intersection of the ITO and the metal electrodes gave an active device area of 4 mm^2. The current density (J), voltage (V) and brightness (B) characteristics of the OLEDs were measured in ambient air with a semiconductor parameter analyzer (E5273A, Agilent) and an optical power meter (1930C, Newport). The EL spectra were recorded using a multi-channel spectrometer (UBS2000, Ocean Optics).

Synthesis

Bis(4-bromophenyl)sulfane (DBDPS). A flame-dried round bottom flask containing a magnetic stirring bar was charged with CuI (0.38 g, 2 mmol), K_2CO_3 (2.76 g, 20 mmol), $Na_2S.9H_2O$ (0.78 g, 10 mmol), 1-bromo-4-iodobenzene (5.65 g, 20 mmol) and DMF (40 mL) under argon atmosphere. The mixture was heated at 120 °C for 18 h and allowed to cool to room temperature. The resulted mixture was extracted with ethyl acetate (3 X 25 mL). The combined organic layers were dried over anhydrous sodium sulphate and concentrated under reduced vacuum. The residue was purified by column chromatography on silica gel with hexane as eluent to give white crystalline solid in 80 % yield (2.80 g). ^{1}H NMR (400 MHz, $CDCl_3$, ppm): δ 7.43 (d, *J* = 8.5 Hz, 4H, Ar-H), 7.18 (d, *J* = 8.5 Hz, 4H, Ar-H). 13C NMR (100 MHz, $CDCl_3$, ppm): δ 134.49, 132.57, 132.43, 121.49.

Bis(4-(phenylethynyl)phenyl)sulfane (DPEDPS). The compound DBDPS (0.68 g, 2 mmol), phenylacetylene (0.5 mL, 4.5 mmol), tetrakis(triphenylphosphine)palladium(0) (0.11 g, 5% mol) and copper(I) iodide (0.07 g, 0.4 mmol) was taken in triethylamine (10 mL). The reaction mixture was stirred at room temperature for 15 min, and then refluxed for overnight under argon atmosphere. The mixture was cooled to room temperature and solvent was evaporated. The residue was directly adsorbed over silica gel and purified by column chromatography with 5 % ethyl acetate/hexane as eluent to give white crystalline solid in 58 % yield (0.45 g). ^{1}H NMR (400 MHz, $CDCl_3$, ppm): δ 7.52 (d, *J* = 3.4 Hz, 4H), 7.47 (d, *J* = 7.7 Hz, 4H), 7.42 – 7.28 (m, 10H). ^{13}C NMR (100 MHz, $CDCl_3$, ppm): δ 135.76, 132.34, 131.62, 130.80, 128.41, 128.38, 123.06, 122.24, 90.47, 88.78. Elemental Analysis ($C_{28}H_{18}S$) Calc. (%): C, 87.01; H, 4.69; S, 8.30. Found (%): C, 87.79; H, 4.47; S, 7.74.

Bis(4-(7,9,10-triphenylfluoranthen-8-yl)phenyl)sulfane (TPFDPS). The compound **TPFDPS** was synthesized from

DPEDPS (0.21 g, 0.55 mmol) and 7,9-diphenyl-8H-cyclopenta[a]acenaphthylen-8-one (DPC) (0.43 g, 1.23 mmol) via Diels-Alder reaction in diphenyl ether (10 mL) as solvent in a sealed tube at 220 °C for 24h. The reaction mixture was subjected to silica gel column chromatography with 10 % ethyl acetate/hexane as eluent to afford greenish-yellow powder in 68% yield (0.38 g). ^{1}H NMR (400 MHz, $CDCl_3$, ppm): δ 7.71 (d, *J* = 8.2 Hz, 4H), 7.30 (dt, *J* = 8.0, 4.7 Hz, 24H), 6.90 (d, *J* = 3.2 Hz, 10H), 6.76 (d, *J* = 8.2 Hz, 4H), 6.66 (d, *J* = 7.1 Hz, 2H), 6.62 (d, *J* = 7.1 Hz, 2H), 6.55 (d, *J* = 8.2 Hz, 4H). ^{13}C NMR (100 MHz, $CDCl_3$, ppm): δ 140.59, 139.99, 139.72, 139.64, 138.67, 137.20, 137.08, 136.71, 136.53, 136.41, 136.38, 133.27, 132.80, 131.89, 131.28, 130.09, 130.07, 129.64, 129.22, 128.23, 128.19, 127.64, 126.96, 126.72, 126.58, 125.46, 123.25, 123.23. Elemental Analysis ($C_{80}H_{50}S$) Calc. (%): C, 92.10; H, 4.83; S, 3.07. Found (%): C, 87.98; H, 4.87; S, 7.11. MS (MALDI-TOF): m/z (%) =1042.44 [M+, ^{32}S, 100 %], 1044.58 [M+, ^{34}S].

2,8-Dibromodibenzothiophene (DBDBT). To a solution of dibenzothiophene (DBT) (5.00 g, 27.1 mmol) in chloroform (30 mL), bromine (3.1 ml, 60.5 mmol) was added dropwise at 0 °C by stirring. Under nitrogen atmosphere the reaction mixture was stirred and kept overnight at room temperature. The crude product was filtered off and washed with methanol to isolate 2,8-dibromodibenzothiophene. The product was obtained as a white powder in 47 % yield (4.40 g). ^{1}H NMR (400 MHz, $CDCl_3$, ppm): δ 8.22 (s, 2H), 7.70 (d, *J* = 8.3 Hz, 2H), 7.57 (d, *J* = 7.6 Hz, 2H). ^{13}C NMR (100 MHz, $CDCl_3$, ppm): δ 138.62, 136.17, 130.29, 124.71, 124.17, 118.62.

2,8-Bis(phenylethynyl)dibenzothiophene (DPEDBT). Same synthesis procedure was followed as mentioned for DPEDPS to give white crystalline solid in 66 % yield (0.75 g). ^{1}H NMR (400 MHz, $CDCl_3$, ppm): δ 8.33 (d, *J* = 1.1 Hz, 2H), 7.81 (s, 1H), 7.79 (s, 1H), 7.63 (d, *J* = 1.5 Hz, 1H), 7.61 (d, *J* = 1.5 Hz, 1H), 7.60 – 7.55 (m, 4H), 7.40 – 7.31 (m, 6H). ^{13}C NMR (100 MHz, $CDCl_3$, ppm): δ 139.71, 135.10, 131.63, 130.13, 128.40, 128.32, 124.91, 123.25, 122.77, 119.76, 89.60, 89.36. Elemental Analysis ($C_{28}H_{16}S$) Calc. (%): C, 87.47; H, 4.19; S, 8.34. Found (%): C, 87.24; H, 4.53; S, 8.23.

2,8-Bis(7,9,10-triphenylfluoranthen-8-yl)dibenzothiophene (TPFDBT). Same synthesis procedure was followed as mentioned for TPFDPS to give greenish powder in 73 % yield (1.0 g). ^{1}H NMR (400 MHz, $CDCl_3$, ppm): δ 7.70 (d, *J* = 8.1 Hz, 4H), 7.45 (d, *J* = 1.2 Hz, 2H), 7.40 – 7.18 (m, 26H), 6.91 (dd, *J* = 8.2, 1.6 Hz, 6H), 6.83 (t, *J* = 12.6 Hz, 6H), 6.61 (dd, *J* = 10.2, 7.1 Hz, 4H). ^{13}C NMR (100 MHz, $CDCl_3$, ppm): δ 140.94, 140.32, 139.80, 139.76, 137.43, 137.29, 136.74, 136.63, 136.45, 135.98, 134.31, 133.29, 131.31, 131.14, 130.03, 129.63, 129.60, 128.27, 128.17, 127.66, 126.93, 126.71, 126.56, 125.44, 124.16, 123.23, 120.79. Elemental Analysis ($C_{80}H_{48}S$) Calc. (%): C, 92.27; H, 4.65; S, 3.08. Found (%): C, 88.53; H, 4.50; S, 6.97. MS (MALDI-TOF): m/z (%) = 1040.45 [M+, 100 %].

Results and Discussion

Synthesis and Characterization

All the fluoranthene derivatives were synthesized as outlined in **Scheme 1**. Bis(4-bromophenyl)sulfane (DBDPS) was synthesized by copper-catalysed C-S bond formation from 1-bromo-4-iodobenzene according to the literature procedure.[43] Bis(4-(phenylethynyl)phenyl)sulfane (PEDPS) was obtained by Sonogashira coupling reaction of DBDPS with phenylacetylene in the presence of CuI and $Pd(PPh_3)_4$ as catalyst and diisopropylamine/toluene as solvent under argon atmosphere. Bis(4-(7,9,10-triphenylfluoranthen-8-yl)phenyl)sulfane (TPFDPS) was obtained by condensation of PEDPS with 7,9-diphenyl-8H-cyclopenta[a]acenaphthylen-8-one (DPC) via Diels-Alder reaction.[38] Following the similar synthetic methods, 2,8-bis(7,9,10-triphenylfluoranthen-8-yl)dibenzo[b,d]thiophene (TPFDBT) was synthesized from dibenzothiophene (DBT).

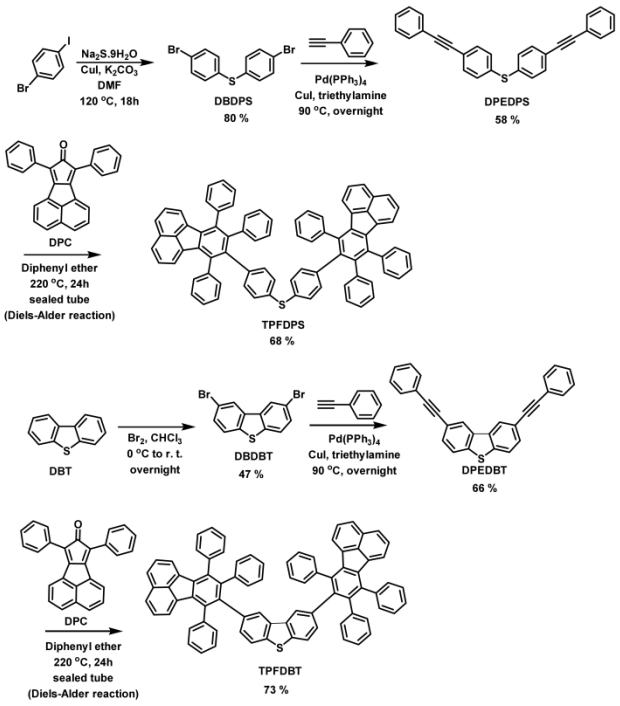

Scheme 1 Synthesis of fluoranthene derivatives

Photophysical Properties

The optical absorption spectra of fluoranthene derivatives in a chloroform solution and thin films are shown in **Figure 1**. Both the compounds in solution and thin film, exhibit two well resolved major intense absorption bands at 299 nm and 375 nm originating from π → π* transitions. There is no significant change observed in absorption spectra of TPFDPS and TPFDBT. The absorption profiles of these fluoranthene derivatives are quite similar in solution and solid states with well resolved vibronic bands in the lower energy region of the spectra. From the low energy onset of the absorption bands, the optical energy gaps were found to be in the range of 3.08-3.09 eV in both thin film and solution. Both fluoranthene derivatives, TPFDPS and TPFDBT, exhibit strong blue emission maxima at 466 nm, 458 nm with a Stoke's shift of 91 nm, 83 nm in

solution, respectively. While a Stoke's shift of 91-92 nm was found in emission maxima of neat films of both the derivatives. A very high PLQY (Φ) of 0.79, and 0.77 was observed in solution with lifetime of 13 ns and 14 ns, while a concentration quenching was noticed in neat films of these derivatives with low PLQY of 0.28 and 0.33 with a lifetime of 11 ns and 7 ns, for TPFDPS and TPFDBT, respectively. Since TPFDPS has an open and flexible structure due to diphenylsulphide (DPS) moiety, particularly in solid state, it can have a planar structure which may lead to aggregation induced quenching of fluorescence in solid state. The lower PLQY in solid state for TPFDPS clearly indicates the concentration quenching effect. On the other hand, in TPFDBT, the rotation is hindered due to steric effect of bulky fluoranthene groups around the more fused and rigid dibenzothiophene (DBT) moiety. As a result, the molecule adopts a non-planar structure in a solid state and fluorescence does not quench effectively as compared to TPFDPS. The photophysical data of both the derivatives is summarized in **Table 1**.

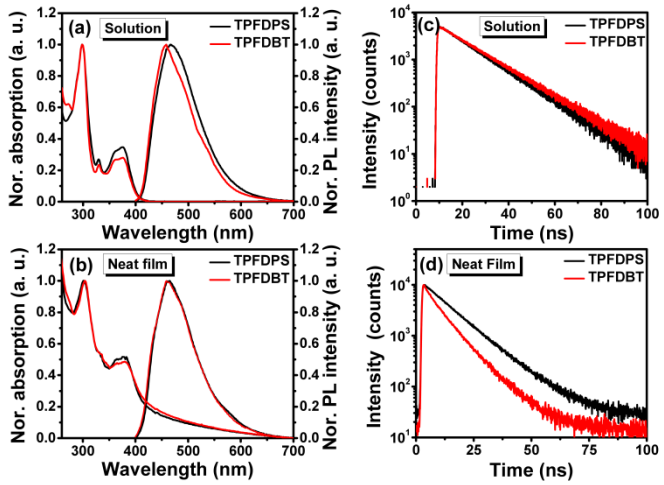

Figure 1 Optical absorption, photoluminescence spectra (a) solution, (b) neat film, and fluorescence lifetime decay (c) solution, (d) neat film of fluoranthene derivatives.

Thermal Stability

Thermal properties and stability of all the fluoranthene derivatives were investigated by differential scanning calorimetry (DSC) and thermogravimetric analysis (TGA), respectively. DSC and TGA curves of fluoranthene derivatives are shown in **Figure 2**. Both the fluoranthene derivatives showed high melting temperature (T_m) and decomposition temperature (T_d). In DSC traces, it can be seen that TPFDPS behaves as the amorphous material with a high T_g of 210 °C and T_m of 348 °C while TPFDBT shows the crystalline nature with T_m of 408 °C (**Figure 2(a, b)** and **(c)**). The crystalline behaviour with high T_m of the TPFDBT is attributed to its more fused and rigid nature of dibenzothiophene (DBT) moiety which implies closed packed structure. Whereas diphenylsulphide (DPS) moiety has open and flexible structure, as a result TPFDPS may adopt a planar structure in the solid state. Both the derivatives are thermally stable up to 495 °C as shown in **Figure 2 (d)**. Thermal characteristic data is summarized in **Table 1**.

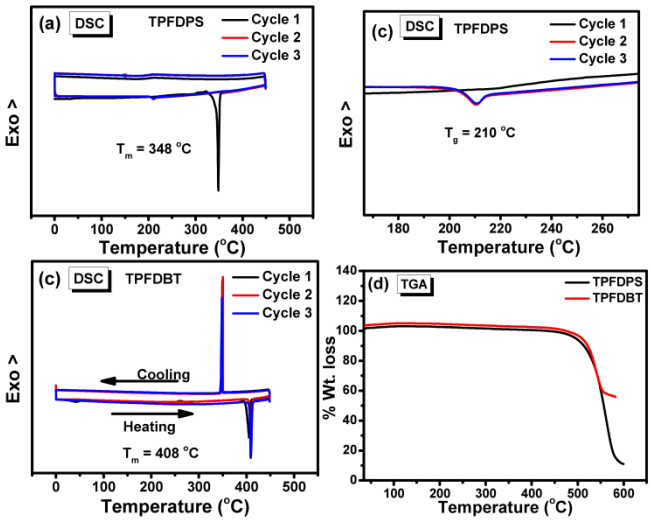

Figure 2 DSC trace of (a, b) TPFDPS and (c) TPFDBT (heating and cooling rate 10 °C/min). (d) TGA curves of TPFDPS and TPFDBT under N_2 atmosphere (Heating rate 5 °C/min)

Electrochemical Properties

The electrochemical stability and energy levels of these fluoranthene derivatives were investigated by cyclic voltammetry (CV). The electrochemical analyzer consists of three electrodes cell with Pt disk as working electrode, Pt wire as counter electrode and Ag/AgCl (saturated with KCl) as a reference electrode. The scan rate was fixed at 50 mV/s. Anhydrous tetrabutylammonium hexafluorophosphate (Bu_4NPF_6) in nitrogen-saturated acetonitrile solvent was used as supporting electrolyte. Ferrocene/ferrocenium (HOMO - 4.80 eV) couple was used as internal standard for calibration of redox potential and calculating the highest occupied molecular. orbital (HOMO) and lowest unoccupied molecular orbital (LUMO) levels.[44] Fluoranthene derivatives were drop-casted on working electrode from dichloromethane solution and both cathodic and anodic sweeps were performed to obtain the redox potentials. The voltammograms obtained from CV measurements are shown in **Figure 3**. The oxidation onset of TPFDPS and TPFDBT were found to be 1.6 V and 1.7 V, respectively. The HOMO energy level calculated with respect to vacuum was found to be -6.1 eV, -6.2 eV, for TPFDPS, TPFDBT, respectively. Such a deep HOMO level of these compounds makes them highly air and electrochemically stable. Similarly, the reduction onset of TPFDPS and TPFDBT was found to be -1.7 V and -1.7 V, respectively. The LUMO energy levels for TPFDPS and TPFDBT calculated with respect to vacuum were found to be -2.8 eV and -2.8 eV, respectively. Also, in the reduction segment, the nature of peak is identified as quasi-reversible in nature, which suggests that these derivatives are capable of stabilizing the anion and electron transport. The electrochemical data is summarized in **Table 2**.

Table 1. Summary of photophysical and thermal properties.

Compound	Solution				Neat film				E_g (eV)	T_g (°C)	T_m (°C)	T_d (°C)
	λ_{abs} (nm)	λ_{em} (nm)	Φ	τ (ns)	λ_{abs} (nm)	λ_{em} (nm)	ϕ	τ (ns)				
TPFDPS	299, 329, 375	466	0.79	13	298, 331, 377	468	0.28	11	3.09	210	495	508
TPFDBT	299, 329, 375	458	0.77	14	298, 331, 377	469	0.33	7	3.08	Not Observed	348	496

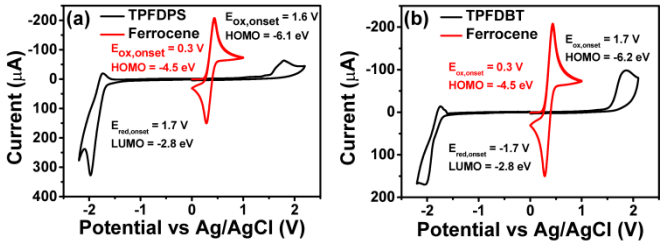

Figure 3 Cyclic voltammograms of (a) TPFDPS and (b) TPFDBT.

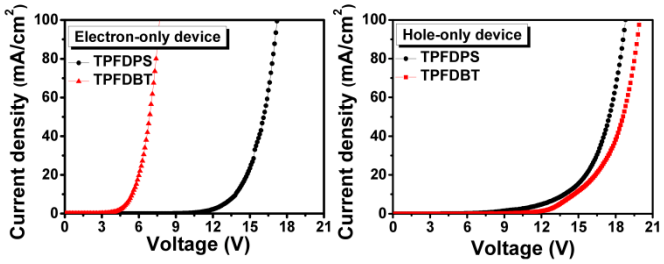

Figure 4 Charge transport characteristics: electron-only device (left), hole-only device (right).

Table 2 Summary of electrochemical properties.

Compound	$E_{oxi,\ onset}$ (V)	HOMO (eV)	$E_{red,\ onset}$ (V)	LUMO (eV)	E_g (eV)
TPFDPS	1.6	-6.1	-1.7	-2.8	3.3
TPFDBT	1.7	-6.2	-1.7	-2.8	3.4

To gain the insight of the charge transport properties of these derivatives, hole-only and electron-only devices were fabricated. The hole-only device fabricated with the following structure: ITO/NPD(10 nm)/fluoranthene derivatives (60 nm)/NPD (10 nm)/Al (100 nm). Similarly, the electron-only device consisted of the following structure: ITO/BPhen (10nm)/fluoranthene derivatives (60 nm)/BPhen (10 nm)/LiF (0.7 nm)/Al (100 nm). NPD (*N,N'*-di(1-naphthyl)-*N,N'*-diphenyl-(*1,1'*-biphenyl)-*4,4'*-diamine) and BPhen (*4,7*-Diphenyl-*1,10*-phenanthroline) were used to prevent injection of an electron from cathode and hole from anode, respectively (**ESI Figure S7**). The charge transport characteristics are shown in **Figure 4**. Although TPFDPS and TPFDBT, both have the same LUMO level, the better electron transport characteristics of TPFDBT attributed can be attributed to its crystalline nature in solid state as observed in the thermal properties. Both the derivatives show poor hole-transport characteristics. The excellent thermal and electron-transport property motivated us to explore the potential of these derivatives as electron transport materials for OLEDs.

Device Characterization

The electron transport properties of these fluoranthene derivatives were demonstrated in organic light emitting diodes. The OLED devices were fabricated with 2-tert-butyl-9,10-bis-(β-naphthyl)-anthracene (TBADN) as a fluorescent emitting material layer (EML) with the following device structure: ITO/TPD (60 nm)/TBADN (10 nm)/ ETL (40 nm)/LiF (1 nm)/Al, where TPD is N,N'-diphenyl-N,N'-bis(3-methylphenyl)(1,1'-biphenyl)-4,4'-diamine, used as a hole transporting layer. The molecular structure of active layers for blue OLEDs fabrication, the energy level diagram, and device architechture is shown in **Figure 5**. Typical light emitting diode EL spectra, current density-voltage (J-V) and luminance-voltage (L-V) characteristics with different ETLs are shown in **Figure 6 (a), (b)** and **6 (c)**, respectively. The position of the peak and shape of EL spectra provides very important information about the exciton recombination region. The peak position of EL spectra of TBADN has shifted to 466±2 nm compared to the reported peak position of PL in thin film is 441 nm.[45] The peak position of EL spectra is same as the peak position of PL spectra of electron transport materials in solid state, but the shape of the EL spectra is significantly different compared to the PL spectra. The energy levels of ETL determined by cyclic voltammetry show the wide band gap; hence we believe that the blue emission originates from TBADN. But, the low EQE values suggest that the charge recombination may take place at the interface of TBADN-ETL , hence we are not ruling out the emission from the interface of TBADN-ETL of the devices. The turn-on voltage of the OLED fabricated with TPFDPS and TPFDBT, was found to be 7.5 V and 6.0 V with the maximum luminance of 212 cd/m^2 and 552 cd/m^2, respectively. The plot of external quantum efficiency-current density (EQE-J) is shown in **Figure 6(d)**. The OLED devices with these

fluoranthene derivatives as ETMs showed the EQE of 0.04 %, and 0.40 % for TPFDPS and TPFDBT, respectively.

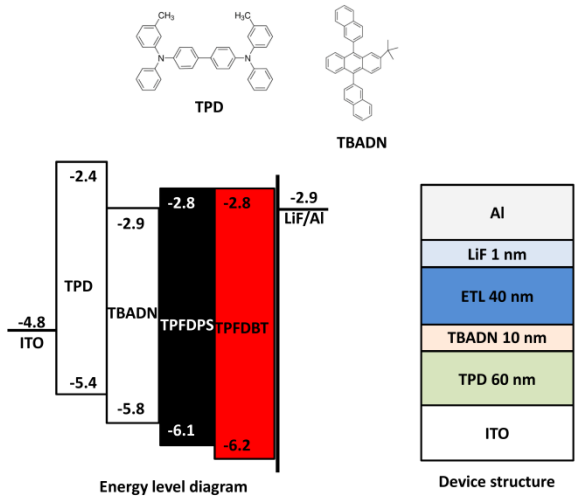

Figure 5 The structure of the chemicals used for fabrication of OLEDs, energy level diagram and device structure.

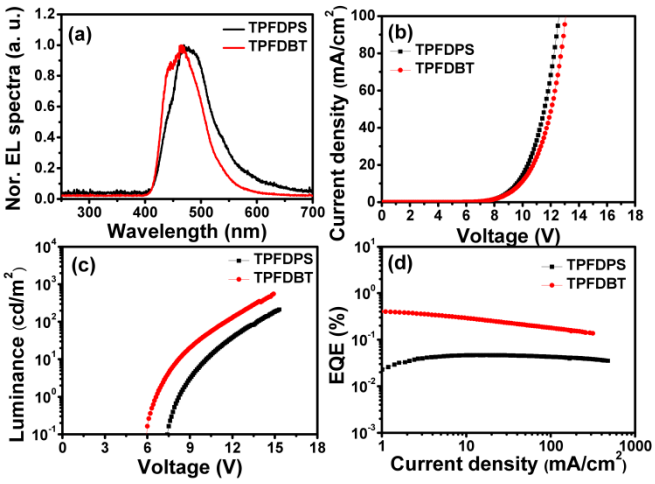

Figure 6 EL spectra of TBADN with TPFDPS and TPFDBT as electron transport layer. (a) J-V characteristics, (b) L-V characteristics, (c) EQE-J characteristics and (d) EL spectra (at 10 mA/cm^2).

Relatively, high turn-on voltage and very low EQE of the device with TPFDPS compared to TPFDBT as ETL can be explained due to its poor electron transport ability and amorphous nature. As it has be observed from the peak position and shape of the EL spectra, there is a poor injection of the electrons from ETL into emitting layer, as a result there is a possibility of electron accumulation at the ETL layer and the charge recombination may take place at the EML-ETL interface.[46] This could possibly limit the device efficiency when we used TPFDPS as ETL layer. On the other hand, TPFDBT being crystalline in nature; transport and inject the electrons into emitting layer more efficiently, thus increasing the overall quantum efficiency. The performance of these devices has not yet been fully optimized. The CIE coordinates of the devices corresponding to the EL spectra are plotted in a chromaticity diagram (**ESI Figure S8**). The EL properties of the devices are summarized in **Table 3**.

Table 3. Summary of electroluminescence properties.

ETL	λ_{EL}(nm)	$V_{turn-on}$ (V)	L_{max}(cd/m^2)	η_{ext}(%)	CIE (x,y)
TPFDPS	468	7.5	212	0.04	(0.13, 0.22)
TPFDBT	464	6.0	552	0.40	(0.13, 0.14)

Conclusions

In conclusion, we have synthesized and characterized two arylated fluoranthene derivatives to study the effect of ring closure on their physical and electronic properties. The observation of electron transport properties with an extremely high Tg for fluoranthene derivatives is unique and important step forward for the development of electron transport materials for OLEDs with high stability and durability. The unusual high melting and glass transition temperature is the major advantage of this new class of materials. These compounds exhibited predominantly electron transport properties as it was evident from the redox properties and the electron-only device characteristics. The electron transport capability of these derivatives as ETM has been explored in blue OLEDs. Further modification to enhance the EQE and reduce the turn-on voltage of OLED by utilizing these derivatives is under progess in our laboratory.

Acknowledgements

Authors thank Prof. Chihaya Adachi and Dr. Qisheng Zhang for useful discussion and providing device fabrication and characterization facility. We thank NMR research centre and Proteomics facility of IISc for NMR and MALDI data. Shiv Kumar acknowledges University Grant Commission (UGC) for a research fellowship.

Notes and references

1. C. W. Tang and S. A. VanSlyke, *Appl. Phys. Lett.*, 1987, **51**, 913-915.
2. K. T. Kamtekar, A. P. Monkman and M. R. Bryce, *Adv. Mater.*, 2010, **22**, 572-582.
3. G. M. Farinola and R. Ragni, *Chem. Soc. Rev.*, 2011, **40**, 3467-3482.
4. A. C. Grimsdale, K. Leok Chan, R. E. Martin, P. G. Jokisz and A. B. Holmes, *Chem. Rev.*, 2009, **109**, 897-1091.
5. A. P. Kulkarni, C. J. Tonzola, A. Babel and S. A. Jenekhe, *Chem. Mater.*, 2004, **16**, 4556-4573.
6. M. Strukelj, F. Papadimitrakopoulos, T. M. Miller and L. J. Rothberg, *Science*, 1995, **267**, 1969-1972.
7. C. Adachi, T. Tsutsui and S. Saito, *Appl. Phys. Lett.*, 1989, **55**, 1489-1491.
8. J. Bettenhausen, P. Strohriegl, W. Brütting, H. Tokuhisa and T. Tsutsui, *J. Appl. Phys.*, 1997, **82**, 4957-4961.
9. C. Adachi, T. Tsutsui and S. Saito, *Appl. Phys. Lett.*, 1990, **56**, 799-801.

10. C. H. Chen and J. Shi, *Coord. Chem. Rev.*, 1998, **171**, 161-174.
11. K. A. Higginson, X.-M. Zhang and F. Papadimitrakopoulos, *Chem. Mater.*, 1998, **10**, 1017-1020.
12. J. Kido, C. Ohtaki, K. Hongawa, K. Okuyama and K. Nagai, *Jpn. J. Appl. Phys.*, 1993, **32**, L917.
13. R. Fink, Y. Heischkel, M. Thelakkat, H.-W. Schmidt, C. Jonda and M. Hüppauff, *Chem. Mater.*, 1998, **10**, 3620-3625.
14. T. D. Anthopoulos, J. P. J. Markham, E. B. Namdas, I. D. W. Samuel, S.-C. Lo and P. L. Burn, *Appl. Phys. Lett.*, 2003, **82**, 4824-4826.
15. M.-Y. Hwang, M.-Y. Hua and S.-A. Chen, *Polymer*, 1999, **40**, 3233-3235.
16. D. O'brien, M. Weaver, D. Lidzey and D. Bradley, *Appl. Phys. Lett.*, 1996, **69**, 881-883.
17. M. Jandke, P. Strohriegl, S. Berleb, E. Werner and W. Brütting, *Macromolecules*, 1998, **31**, 6434-6443.
18. B. W. D'Andrade, S. R. Forrest and A. B. Chwang, *Appl. Phys. Lett.*, 2003, **83**, 3858-3860.
19. C. Adachi, M. A. Baldo, S. R. Forrest and M. E. Thompson, *Appl. Phys. Lett.*, 2000, **77**, 904-906.
20. S. B. Heidenhain, Y. Sakamoto, T. Suzuki, A. Miura, H. Fujikawa, T. Mori, S. Tokito and Y. Taga, *J. Am. Chem. Soc.*, 2000, **122**, 10240-10241.
21. Y. Sakamoto, T. Suzuki, A. Miura, H. Fujikawa, S. Tokito and Y. Taga, *J. Am. Chem. Soc.*, 2000, **122**, 1832-1833.
22. T. Noda and Y. Shirota, *J. Am. Chem. Soc.*, 1998, **120**, 9714-9715.
23. N. Camaioni, G. Ridolfi, V. Fattori, L. Favaretto and G. Barbarella, *Appl. Phys. Lett.*, 2004, **84**, 1901-1903.
24. T. H. Huang, W. T. Whang, J. Y. Shen, Y. S. Wen, J. T. Lin, T. H. Ke, L. Y. Chen and C. C. Wu, *Adv. Funct. Mater.*, 2006, **16**, 1449-1456.
25. M. M. Alam and S. A. Jenekhe, *Chem. Mater.*, 2002, **14**, 4775-4780.
26. P. Lu, H. Hong, G. Cai, P. Djurovich, W. P. Weber and M. E. Thompson, *J. Am. Chem. Soc.*, 2000, **122**, 7480-7486.
27. Y. Liu, H. Ma and A. K. Jen, *Chem. Mater.*, 1999, **11**, 27-29.
28. S. C. Lo, N. A. H. Male, J. P. J. Markham, S. W. Magennis, P. L. Burn, O. V. Salata and I. D. W. Samuel, *Adv. Mater.*, 2002, **14**, 975-979.
29. J. Bettenhausen, M. Greczmiel, M. Jandke and P. Strohriegl, *Synth. Met.*, 1997, **91**, 223-228.
30. F. Wang, J. Hu, X. Cao, T. Yang, Y. Tao, L. Mei, X. Zhang and W. Huang, *J. Mater. Chem. C*, 2015, DOI: 10.1039/c5tc00350d.
31. C.-H. Shih, P. Rajamalli, C. A. Wu, W.-T. Hsieh and C.-H. Cheng, *ACS Appl. Mater. Interfaces*, 2015, DOI: 10.1021/acsami.5b01872.
32. S. H. Tucker and M. Whalley, *Chem. Rev.*, 1952, **50**, 483-538.
33. E. W. Thulstrup and J. Eggers, *Chem. Phys. Lett.*, 1968, **1**, 690-692.
34. J. Kolc, E. W. Thulstrup and J. Michl, *J. Am. Chem. Soc.*, 1974, **96**, 7188-7202.
35. A. Goel, V. Kumar, S. Chaurasia, M. Rawat, R. Prasad and R. S. Anand, *J. Org. Chem.*, 2010, **75**, 3656-3662.
36. I. B. Berlman, H. O. Wirth and O. J. Steingraber, *J. Am. Chem. Soc.*, 1968, **90**, 566-569.
37. H. Güsten and G. Heinrich, *J. Photochem.*, 1982, **18**, 9-17.
38. R. C. Chiechi, R. J. Tseng, F. Marchioni, Y. Yang and F. Wudl, *Adv. Mater.*, 2006, **18**, 325-328.
39. S. K. Kim, J. Y. Jaung and J. W. Park, *Mol. Cryst. Liq. Cryst.*, 2008, **491**, 122-132.
40. S. K. Kim and J. W. Park, *J. Nanosci. Nanotech.*, 2008, **8**, 4787-4792.
41. Y. Zhou, L. Ding, K. Shi, Y. Z. Dai, N. Ai, J. Wang and J. Pei, *Adv. Mater.*, 2012, **24**, 957-961.
42. C. M. Cardona, W. Li, A. E. Kaifer, D. Stockdale and G. C. Bazan, *Adv. Mater.*, 2011, **23**, 2367-2371.
43. Y. Li, C. Nie, H. Wang, X. Li, F. Verpoort and C. Duan, *Eur. J. Org. Chem.*, 2011, **2011**, 7331-7338.
44. M. Thelakkat and H. W. Schmidt, *Adv. Mater.*, 1998, **10**, 219-223.
45. S. Tao, Z. Hong, Z. Peng, W. Ju, X. Zhang, P. Wang, S. Wu and S. Lee, *Chem. Phys. Lett.*, 2004, **397**, 1-4.
46. K. Itano, H. Ogawa and Y. Shirota, *Appl. Phys. Lett.*, 1998, **72**, 636-638.